**Reports in Mechanical Engineering**
Vol. 1, No. 1, 2020, pp. 141-150.
ISSN: 2683-5894, DOI: https://doi.org/10.31181/rme200101141v 

# Free vibration of simply supported steel I-girders with trapezoidal web corrugations

**Duy-Quang Vo [1] and Hoang Lan Ton-That [1*]**
[1] Department of Civil Engineering, University of Architecture Ho Chi Minh City, Vietnam, e-mail: lan.tonthathoang@uah.edu.vn

**Article Info**

***Article history:***

Received October 28, 2020
Revised November 28, 2020
Accepted December 1, 2020

***Keywords:***

Natural frequency;
Trapezoidal web corrugations;
I-girder;
Stiffness matrix;
Mass matrix.

**ABSTRACT**

Natural frequency is essential information required to perform the dynamic analysis. In this study, the straight I-girder element with trapezoidal web corrugations and singly symmetric cross-section is derived based on Kang and Yoo's thin-walled curved beam with doubly symmetric cross-section theory. Each node of the element has seven degrees of freedom including one warping degree of freedom. Using Hamilton's principle, governing linear dynamic differential equations of equilibrium, elastic element stiffness matrix, and consistent element mass matrix are established. Matlab code is employed for natural frequency analysis of simply supported steel I-girders with trapezoidal web corrugations. The results are compared with the natural frequencies obtained with ABAQUS. Finally, it is found that the proposed equations provide a good prediction of natural frequency for the first three lateral bending modes and the first five torsional modes.



***Corresponding Author:***

Hoang Lan Ton-That,
Department of Civil Engineering, University of Architecture Ho Chi Minh City, Vietnam.
Email: lan.tonthathoang@uah.edu.vn

## 1. Introduction

The straight I-girders with trapezoidal web corrugations have been widely used in many different structures, primarily bridge constructions and civil steel structures since the early 1960s in Europe (Abbas, 2003). They have many advantages that can be listed here: *(i)* the corrugated steel webs can be used to replace the synergistic effect of the flat steel plates of the conventional I-girders and reinforced steel plates; *(ii)* resulting in stiffer I-girders with trapezoidal web corrugations when flexed out of the plane, the torsional resistance is better; *(iii)* reducing the cost of fabrication by reducing the weight of steel; and *(iv)* improving the attractiveness of structural design. (Lindner, 1990), (Sayed-Ahmed, 2005), (Moon *et al.*, 2009) studied the elastic lateral-torsional buckling strength of an I-girder with trapezoidal web corrugations ($M_{cr}$). All three studies stem from the determination of the warping constant $C_{w,C}$. Specifically, (Lindner, 1990) determined $C_{w,C}$ based on the experimental formula. (Sayed-Ahmed, 2005) determined $C_{w,C}$ by replacing the corrugated steel web with a flat steel plate of equal thickness but without a specific theoretical basis. Besides, (Moon *et al.*, 2009) used the force method to investigate the influence of the web plate and wing plate, thereby calculating $C_{w,C}$. After finding $C_{w,C}$, all three studies used the same formula to calculate $M_{cr}$. The disadvantage of all three studies is that the geometries of the cross-section have not been completely resolved, so they cannot give a sufficiently accurate result for $C_{w,C}$, and $M_{cr}$. This is only completely resolved based on the research of (Nguyen *et al.*, 2010). These authors studied the cross-sectional geometry of a straight I-girder with trapezoidal web corrugations and calculated $M_{cr}$. (Nguyen *et al.*, 2010) used the calculus equations to find $C_{w,C}$, and $M_{cr}$. The results of $M_{cr}$ found analytically were compared with the results of finite element method (FEM) and previous studies by (Lindner, 1990), (Sayed-Ahmed, 2005), (Moon *et al.*, 2009) and with $M_{cr}$ of I-girder with flat steel plate. The highlight of (Nguyen *et al.*, 2010) is that for the first time, the general formulas for the cross-sectional geometry of an I-girder with trapezoidal web corrugations have been found, thereby finding $C_{w,C}$ and $M_{cr}$ with accuracy higher than previous studies. Furthermore, (Kövesdi *et al.*, 2016) studied the bending and shear behavior of I-girder with trapezoidal web corrugations. (Kövesdi *et al.*, 2016) focused on investigating the influence of corrugated steel web on the lateral bending moment in the flange plane and the load-bearing capacity of girders. (Jager *et al.*, 2017) used the experimental results to study the flange buckling behavior of I-girder with trapezoidal web corrugations. They introduced an additional experimental research program to investigate the flange buckling behavior and the bending moment resistance of girders. (Riahi *et al.*, 2018) studied the shear buckling of I-girder with the flat web and the trapezoidal, sinusoidal, and zigzag web corrugations. (Riahi *et al.*, 2018) said that the damage of the beam is due to the shear buckling of the web without any interaction of the flange. (Riahi *et al.*, 2018) based on the results of the nonlinear analysis showed that shear stress was the largest and evenly distributed on the web before the buckling. In addition, after buckling, the shear stress was reduced and not evenly distributed. (Lin *et al.*, 2019) studied the mechanical properties and behavior of I-girder with corrugated webs. I-girder with corrugated webs was quite commonly used in Australia, but the information about their mechanical properties is not available. They developed a set of I-girder with corrugated webs data on the size and mechanical properties for use in practical applications in Australia. (Inaam *et al.*, 2020) studied the behavior of I-girder with corrugated webs under patch loading by the method of changing parameters. (Inaam et al., 2020) investigated the change of loading and geometric parameters to study the behavior of I-girder with corrugated webs. Finally, based on the results of the numerical survey, they also developed an experimental model to determine the extreme patch load-bearing capacity of the cantilever-shaped I-girder with corrugated webs. Besides, the strength of finite element analyses (Ton et al., 2017, 2018, 2020) as well as commercial software also contribute to the development of analysis of structures with optimal shape.

Natural frequency is essential information required to perform the dynamic analysis. Understanding the natural frequency will be a prerequisite to avoid undesirable vibrations that can occur in steel girders under a load of vehicles and trains. This paper uses Kang and Yoo's thin-walled curved beam with doubly symmetric cross-section theory as in (Kang et al., 1994) to derive the variational and finite-element formulas for the straight I-girder element with trapezoidal web corrugations and singly symmetric cross-section as shown in Figure 1. Each node of the element has seven degrees of freedom including one warping degree of freedom. Using Hamilton's principle, governing linear dynamic differential equations of equilibrium, elastic element stiffness matrix, and consistent element mass matrix are derived. Matlab code is employed for natural frequency analysis of simply supported steel I-girders with trapezoidal web corrugations. The results are compared with the natural frequencies using ABAQUS software. Finally, it is found that the proposed equations provide a good prediction of natural frequency for the first three lateral bending modes and the first five torsional modes.

## 2. Variational formulation for linear dynamic analysis – equation of motion

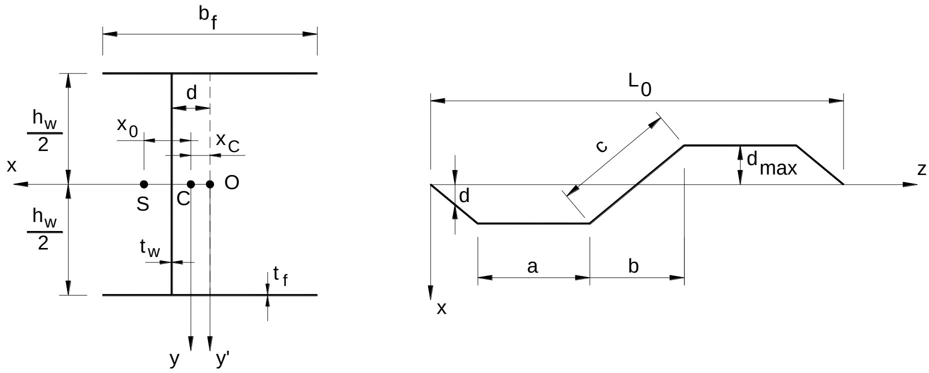


(a) (b)

**Figure 1.** (a) Dimensions of cross-section, (b) Dimensions of corrugation profiles of I-girder with trapezoidal web corrugations

Using Hamilton's principle, the dynamic equation of equilibrium can be expressed in the following variational form

$$\int_{t_1}^{t_2} \left(\delta T + \delta U + \delta\Omega\right) dt = 0 \tag{1}$$

in which $\delta T$ is variation of kinetic energy, $\delta U$ is variation of strain energy, $\delta\Omega$ is variation of loss of potential energy due to applied loads and $t$ denotes time.

By substituting the strain - displacement relationship and the stress resultant - displacement relationship into Eq. (1) and conducting the variational calculation, we obtain the governing linear dynamic differential equations

$$EI_y u_0^{IV} + \rho A\ddot{u}_0 - \rho I_y \ddot{u}_0^{"} = q_x - m_y^{'} \tag{2-a}$$

$$EI_x v_0^{IV} + EI_{y\omega}\beta^{IV} + \rho A\ddot{v}_0 - \rho A x_0 \ddot{\beta} - \rho I_x \ddot{v}_0^{"} - \rho I_{y\omega}\ddot{\beta}^{"} = q_y + m_x^{'} \tag{2-b}$$

$$-EAw_0^{"} + \rho A\ddot{w}_0 = q_z \tag{2-c}$$

$$EI_{y\omega}v_0^{IV} + EI_\omega\beta^{IV} - GK_T\beta^{"} + \rho I_x\ddot{\beta} - \rho A x_0\ddot{v}_0 + \rho\left(I_y + x_0^2 A\right)\ddot{\beta} - \rho I_{y\omega}\ddot{v}_0^{"} - \rho I_\omega\ddot{\beta}^{"} = m_z + m_\omega^{'} \tag{2-d}$$

where $u_0$, $v_0$, $w_0$ and $\beta$ are the displacements in $x$, $y$, $z$ directions and the rotation angle around the $z$-axis of the shear center $S$, respectively; $x_0$ is the $x$-coordinate of the shear center $S$ for the axis system passing through the center of gravity $Cxy$, $\rho$ is the density, $E$ is Young's modulus of elasticity, $G$ is the shear modulus of elasticity, $K_T$ is the Saint-Venant twist constant, $A$ is the cross-section area. $I_x$, $I_y$, $I_\omega$ are the moments of inertia for the $x$-axis, $y$-axis, and warping, respectively. $I_{y\omega}$ is the cross-section geometry. $q_x$, $q_y$, $q_z$, $m_x$, $m_y$, $m_z$, $m_\omega$ are the uniformly distributed force along the $x$-axis, $y$-axis, $z$-axis, the uniformly distributed moment along the $x$-axis, $y$-axis, $z$-axis, and the uniformly distributed bimoment, respectively. Looking at Eqs. (2a)-(2d), we see that there are three displacement fields behaving completely independently of each other. $u_0$ is the horizontal displacement, $w_0$ is the axial displacement and the displacement field ($v_0$ and $\beta$) is the vertical displacement and the torsional displacement. This is a very important feature, it makes up the completely separate behavior of the three displacement fields as given above.

## 3. Finite element formulation for linear dynamic analysis

The result of applying Hamilton's principle is written in the matrix form as follows

$$\delta T + \delta U + \delta\Omega = \delta\mathbf{d}^{\mathbf{T}}(\mathbf{M}\mathbf{d} + \mathbf{K}\mathbf{d} - \mathbf{f}) = 0 \tag{3}$$

resulting in:

$$\mathbf{M}\mathbf{d} + \mathbf{K}\mathbf{d} - \mathbf{f} = \mathbf{0} \tag{4}$$

where **K**, **M**, **d** and **f** are the linear stiffness matrix, consistent mass matrix, nodal displacement vector and applied force vector of a global structural system.

Nodal forces and nodal displacements are also shown in Figure 2. The nodal forces are the stress resultants $F_z$, $M_y$, $M_x$, $B_i$, $T_T$, $V_x$ and $V_y$. The nodal displacements $w_0$, $\gamma$, $-v_0^{'}$, $-\tau$, $\beta$, $u_0$ and $v_0$, have the same directions as those of the stress resultants $F_z$, $M_y$, $M_x$, $B_i$, $T_T$, $V_x$ and $V_y$, respectively, with

$$\gamma = u_0^{'} \tag{5-a}$$

and

$$\tau = \beta^{'} \tag{5-b}$$

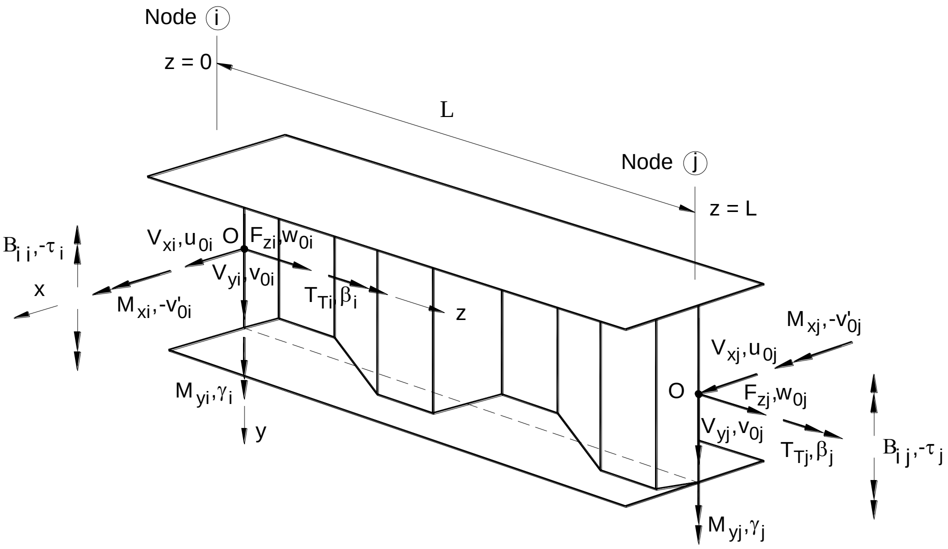


**Figure 2.** Geometry of a element

Because there are three independent displacement fields: ($u_0$ and $\gamma$), ($w_0$) and ($v_0$, $-v'_0$, $-\tau$ and $\beta$), so we define the element nodal displacement vectors and the element nodal force vectors in the following form

$$\mathbf{d} = [\,\mathbf{d}^{\mathbf{u}\,T} \;\; \mathbf{d}^{\mathbf{w}\,T} \;\; \mathbf{d}^{\mathbf{out}\,T}\,]^T = d_k\,, \;\; k = 1, 2, \ldots, 14 \tag{6-a}$$

$$\mathbf{f} = [\,\mathbf{f}^{\mathbf{u}\,T} \;\; \mathbf{f}^{\mathbf{w}\,T} \;\; \mathbf{f}^{\mathbf{out}\,T}\,]^T = f_k\,, \quad k = 1, 2, \ldots, 14 \tag{6-b}$$

where

$$\mathbf{d}^{\mathbf{u}} = [\,u_{0i} \;\; \gamma_i \;\; u_{0j} \;\; \gamma_j\,]^T = d_k^u\,, \quad k = 1, 2, 3, 4 \tag{7-a}$$

$$\mathbf{d}^{\mathbf{w}} = [\,w_{oi} \;\; w_{oj}\,]^T = d_k^w\,, \quad k = 5, 6 \tag{7-b}$$

$$\mathbf{d}^{\mathbf{out}} = [\,v_{oi} \;\; -v'_{0i} \;\; \beta_i \;\; -\tau_i \;\; v_{oj} \;\; -v'_{0j} \;\; \beta_j \;\; -\tau_j\,]^T = d_k^{out}\,, \;\; k = 7, 8, \ldots, 14 \tag{7-c}$$

$$\mathbf{f}^{\mathbf{u}} = [\,V_{xi} \;\; M_{yi} \;\; V_{xj} \;\; M_{yj}\,]^T = f_k^u\,, \;\; k = 1, 2, 3, 4 \tag{7-d}$$

$$\mathbf{f}^{\mathbf{w}} = [\,F_{zi} \;\; F_{zj}\,]^T = f_k^w\,, \;\; k = 5, 6 \tag{7-e}$$

$$\mathbf{f}^{\mathbf{out}} = [\,V_{yi} \;\; M_{xi} \;\; T_{Ti} \;\; B_{i\,i} \;\; V_{yj} \;\; M_{xj} \;\; T_{Tj} \;\; B_{i\,j}\,]^T = f_k^{out}\,, \quad k = 7, 8, \ldots, 14 \tag{7-f}$$

where the subscripts " i " and " j " denote the node numbers and the superscript " T " denotes transpose. $\mathbf{d}^{\mathbf{u}}$, $\mathbf{d}^{\mathbf{w}}$, $\mathbf{d}^{\mathbf{out}}$ are the components according to *u* (along the *x*-axis), *w* (along the *z*-axis) and out-of-plane of the vector **d**, respectively. $\mathbf{f}^{\mathbf{u}}$, $\mathbf{f}^{\mathbf{w}}$, $\mathbf{f}^{\mathbf{out}}$ are the components according to *u* (along the *x*-axis), *w* (along the *z*-axis) and out-of-plane of the vector **f**. Next, the displacement fields can be expressed in terms of nodal displacements by the shape function

$$\mathbf{u} = \mathbf{N}\,\mathbf{d} \tag{8}$$

in which

$$\mathbf{u} = [u_0 \;\; w_0 \;\; v_0 \;\; \beta\,]^T = [\,\mathbf{u}^{\mathbf{u}\,T} \;\; \mathbf{u}^{\mathbf{w}\,T} \;\; \mathbf{u}^{\mathbf{out}\,T}\,]^T = u_k\,, \;\; k = 1, 2, 3, \tag{9-a}$$

$$\mathbf{u}^{\mathbf{u}} = [\,u_0\,]^T = [\,u_1\,]^T = u_k\,, \;\; k = 1 \tag{9-b}$$

$$\mathbf{u}^{\mathbf{w}} = [w_0\,]^T = [\,u_2\,]^T = u_k\,, \;\; k = 2 \tag{9-c}$$

$$\mathbf{u}^{\mathbf{out}} = [v_0 \;\; \beta\,]^T = [\,u_3 \;\; u_4\,]^T = u_k\,, \;\; k = 3, 4 \tag{9-d}$$

and $\mathbf{u}^{\mathbf{u}}$, $\mathbf{u}^{\mathbf{w}}$, $\mathbf{u}^{\mathbf{out}}$ are the components according to *u* (along the *x*-axis), *w* (along the *z*-axis) and out-of-plane of the displacement field **u**. In this paper, we first give the formulas of the shape function **N** as follows

$$\mathbf{N}=\begin{bmatrix}\mathbf{N}^{\mathbf{u}}_{(1\times4)} & & \mathbf{0}\\ & \mathbf{N}^{\mathbf{w}}_{(1\times2)} & \\ \mathbf{0} & & \mathbf{N}^{\mathbf{out}}_{(2\times8)}\end{bmatrix} \tag{10-a}$$

$$\mathbf{N}^{\mathbf{u}}=\left[1-3\xi^2+2\xi^3 \quad L\left(\xi-2\xi^2+\xi^3\right) \quad 3\xi^2-2\xi^3 \quad L\left(-\xi^2+\xi^3\right)\right] \tag{10-b}$$

$$\mathbf{N}^{\mathbf{w}}=\left[1-\xi \quad \xi\right] \tag{10-c}$$

$$\mathbf{N}^{\mathbf{out}}=\begin{bmatrix}H_3 & H_1 & 0 & 0 & H_4 & H_2 & 0 & 0\\ 0 & 0 & H_3 & H_1 & 0 & 0 & H_4 & H_2\end{bmatrix}=\begin{bmatrix}\mathbf{N_{out1}}\\ \mathbf{N_{out2}}\end{bmatrix} \tag{10-d}$$

where $\mathbf{N^u}$, $\mathbf{N^w}$, $\mathbf{N^{out}}$ are the components according to *u* (along the *x*-axis), *w* (along the *z*-axis) and out-of-plane of the shape function **N**, and:

$$H_1=\frac{\alpha_1L-e^{2\alpha_1L}+\alpha_1Le^{2\alpha_1L}+1}{H_5}-\frac{e^{\alpha_1z}\left(\alpha_1L-e^{\alpha_1L}+1\right)}{H_5}+\frac{z\left(e^{\alpha_1L}-1\right)}{H_6}-\frac{e^{\alpha_1L}e^{(-\alpha_1z)}\left(\alpha_1Le^{\alpha_1L}-e^{\alpha_1L}+1\right)}{H_5} \tag{10-d1}$$

$$H_2=-\frac{2\alpha_1Le^{\alpha_1L}-e^{2\alpha_1L}+1}{H_5}+\frac{e^{\alpha_1z}\left(\alpha_1Le^{\alpha_1L}-e^{\alpha_1L}+1\right)}{H_5}+\frac{z\left(e^{\alpha_1L}-1\right)}{H_6}+\frac{e^{\alpha_1L}e^{(-\alpha_1z)}\left(\alpha_1L-e^{\alpha_1L}+1\right)}{H_5} \tag{10-d2}$$

$$H_3=\frac{\alpha_1L-e^{\alpha_1L}+\alpha_1Le^{\alpha_1L}+1}{H_6}+\frac{e^{\alpha_1z}}{H_6}-\frac{e^{\alpha_1L}e^{(-\alpha_1z)}}{H_6}-\frac{z\left(\alpha_1+\alpha_1e^{\alpha_1L}\right)}{H_6} \tag{10-d3}$$

$$H_4=-H_3+\frac{\alpha_1L-2e^{\alpha_1L}+\alpha_1Le^{\alpha_1L}+2}{H_6} \tag{10-d4}$$

$$H_5=2\alpha_1-4\alpha_1e^{\alpha_1L}+2\alpha_1e^{2\alpha_1L}+\alpha_1^2L-\alpha_1^2Le^{2\alpha_1L} \tag{10-d5}$$

$$H_6=\alpha_1L-2e^{\alpha_1L}+\alpha_1Le^{\alpha_1L}+2 \tag{10-d6}$$

$$\alpha_1=\sqrt{\frac{EI_xGK_T}{EI_xEI_\omega-\left(EI_{y\omega}\right)^2}} \tag{10-d7}$$

$$\xi = z/L \tag{10-e}$$

### 3.1. Elastic element stiffness matrix $\mathbf{K_e}$

The formula of the elastic element stiffness matrix $\mathbf{K_e}$ is given as:

$$\mathbf{K_e}=\begin{bmatrix}\mathbf{K}^{\mathbf{u}}_{\mathbf{e}(4\times4)} & & \mathbf{0}\\ & \mathbf{K}^{\mathbf{w}}_{\mathbf{e}(2\times2)} & \\ \mathbf{0} & & \mathbf{K}^{\mathbf{out}}_{\mathbf{e}(8\times8)}\end{bmatrix} \tag{11}$$

in which $\mathbf{K^u_e}$, $\mathbf{K^w_e}$, $\mathbf{K^{out}_e}$ are the components according to *u* (along the *x*-axis), *w* (along the *z*-axis) and out-of-plane of the elastic element stiffness matrix $\mathbf{K_e}$

$$K^u_{eij}=EI_y\int_L N''_{ui}N''_{uj}dz\text{ ; i, j = 1, 2, 3, 4} \tag{12}$$

$$K^w_{eij}=EA\int_L N'_{wi}N'_{wj}dz\text{ ; i, j = 5,} \tag{13}$$

$$K_{eij}^{out} = EI_x \int_L N''_{out1i} N''_{out1j} dz + EI_{y\omega} \int_L \left( N''_{out1i} N''_{out2j} + N''_{out1j} N''_{out2i} \right) dz +$$

$$EI_\omega \int_L N''_{out2i} N''_{out2j} dz + GK_T \int_L N'_{out2i} N'_{out2j} dz \tag{14}$$

$$i, j = 7, 8, ..., 14$$

### 3.2. Consistent element mass matrix $\mathbf{M_e}$

The consistent element mass matrix $\mathbf{M_e}$ has the following form:

$$\mathbf{M_e} = \begin{bmatrix} \mathbf{M}^{\mathbf{u}}_{\mathbf{e}(4\times4)} & & \mathbf{0} \\ & \mathbf{M}^{\mathbf{w}}_{\mathbf{e}(2\times2)} & \\ \mathbf{0} & & \mathbf{M}^{\mathbf{out}}_{\mathbf{e}(8\times8)} \end{bmatrix} \tag{15}$$

in which $\mathbf{M}^{\mathbf{u}}_{\mathbf{e}}$, $\mathbf{M}^{\mathbf{w}}_{\mathbf{e}}$, $\mathbf{M}^{\mathbf{out}}_{\mathbf{e}}$ are the components according to $u$ (along the $x$-axis), $w$ (along the $z$-axis) and out-of-plane of the consistent element mass matrix $\mathbf{M_e}$

$$M_{eij}^{u} = \rho A \int_L N_{ui} N_{uj} dz + \rho I_y \int_L N'_{ui} N'_{uj} dz \text{ ; i, j = 1, 2, 3, 4} \tag{16}$$

$$M_{eij}^{w} = \rho A \int_L N_{wi} N_{wj} dz \text{ ; i, j = 5, 6} \tag{17}$$

$$M_{eij}^{out} = \rho A \int_L \left[ N_{out1i} N_{out1j} - x_0 \left( N_{out1i} N_{out2j} + N_{out1j} N_{out2i} \right) + x_0^2 N_{out2i} N_{out2j} \right] dz + \rho I_y \int_L N_{out2i} N_{out2j} dz +$$
$$+ \rho I_x \int_L \left( N_{out2i} N_{out2j} + N'_{out1i} N'_{out1j} \right) dz + \rho I_{y\omega} \int_L \left( N'_{out1i} N'_{out2j} + N'_{out1j} N'_{out2i} \right) dz + \rho I_\omega \int_L N'_{out2i} N'_{out2j} dz \tag{18}$$

with i, j = 7, 8, …, 14

## 4. Examples

Natural frequencies are obtained as a result of the eigenvalue problem:

$$\left( [\mathbf{K}] - \omega^2 [\mathbf{M}] \right) \{\mathbf{q}\} = \{\mathbf{0}\} \tag{19}$$

The natural frequency formulas for simply supported steel I-girder with trapezoidal web corrugations according to the BL-lateral bending modes and the T-torsional modes are proposed here:

$$\omega_{BL}^{n} = \frac{n^2\pi^2}{L^2} \sqrt{\frac{EI_y}{\rho A \left( 1 + \frac{n^2\pi^2}{L^2} \times \frac{I_y}{A} \right)}} \text{ ; n = 1, 2, 3} \tag{20}$$

$$\omega_{T}^{n} = \frac{n\pi}{L} \sqrt{\frac{\left( \frac{n^2\pi^2}{L^2} EI_\omega + GK_T \right)}{\rho \left( I_x + I_y \right) \left( 1 + \frac{n^2\pi^2}{L^2} \times \frac{I_y + I_\omega + \alpha_n I_{y\omega}}{A} \right)}} \text{ ; n = 1, 2, 3,4,5} \tag{21}$$

with $\alpha_1 = 300$, $\alpha_2 = 100$, $\alpha_3 = 48$, $\alpha_4 = 27$, $\alpha_5 = 18$.

To check the correctness of the proposed Eqs. (20) and (21), we calculate the natural frequencies of three simply supported steel I-girders with trapezoidal web corrugations and with dimensions as given in Table 1. The material properties are taken with the Young's modulus $E = 2\times10^5$ N/mm$^2$, shear modulus $G=E/[2(1+\upsilon)]$, Poisson's ratio $\upsilon$=0.3 and density $\rho$=7850 kg/m$^3$. Three different solutions are presented as follows:

1. Using four-node shell elements (S4R) to simulate three B1 ÷ B3 beams by using ABAQUS software as shown in Figures 3÷12.

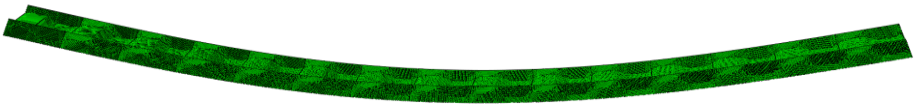

**Figure 3.** The first lateral bending mode ($BL_1$) of the B3 beam uses the shell-S4R element

**Figure 4.** The second lateral bending mode ($BL_2$) of the B3 beam uses the shell-S4R element

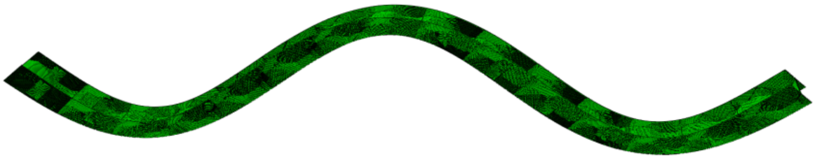

**Figure 5.** The third lateral bending mode ($BL_3$) of the B3 beam uses the shell-S4R element

**Figure 6.** The first vertical bending mode ($BV_1$) of the B3 beam uses the shell-S4R element

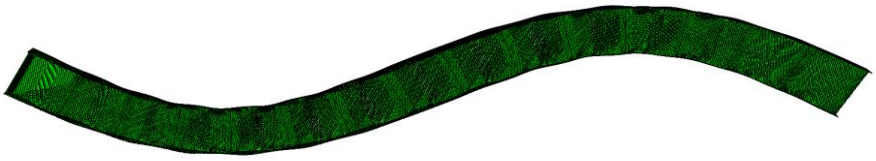

**Figure 7.** The second vertical bending mode ($BV_2$) of the B3 beam uses the shell-S4R element

**Figure 8.** The first torsional mode ($T_1$) of the B3 beam uses the shell-S4R element

**Figure 9.** The second torsional mode ($T_2$) of the B3 beam uses the shell-S4R element

**Figure 10.** The third torsional mode ($T_3$) of the B3 beam uses the shell-S4R element

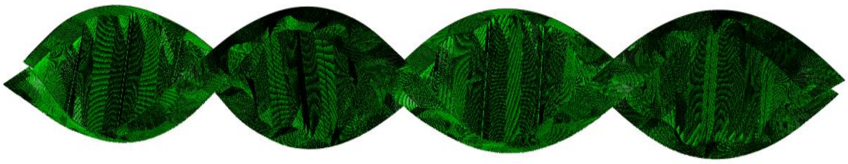

**Figure 11.** The fourth torsional mode ($T_4$) of the B3 beam uses the shell-S4R element

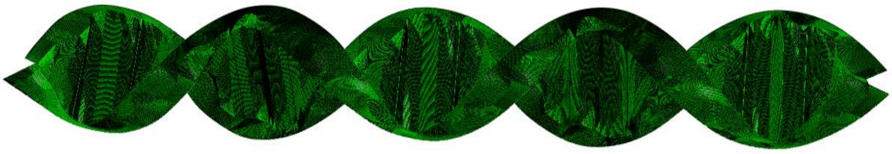

**Figure 12.** The fifth torsional mode ($T_5$) of the B3 beam uses the shell-S4R element

2. Using the beam element with seven degrees of freedom (7DOFs beam element) for each node and with the matrix $\mathbf{K_e}$ from Eq. (11) as well as $\mathbf{M_e}$ from Eq. (15), the authors analyze the natural frequency for the three beams B1 ÷ B3 obtained with the Matlab code and compare to the FE results.
3. Using the authors' proposed formulas to calculate the natural frequency values for three beams B1 ÷ B3 according to Eqs. (20) and (21).

**Table 1.** Geometry data of three analysis models.

| Model | a (mm) | b (mm) | $d_{max}$ (mm) | c (mm) | $t_w$ (mm) | $h_w$ (mm) | $b_f$ (mm) | $t_f$ (mm) | L (mm) |
|---|---|---|---|---|---|---|---|---|---|
| B1 | 250 | 200 | 30 | 208.81 | 8 | 1000 | 400 | 25 | 13500 |
| B2 | 250 | 200 | 45 | 219.32 | 8 | 1000 | 400 | 25 | 13500 |
| B3 | 250 | 200 | 60 | 233.24 | 8 | 1000 | 400 | 25 | 13500 |

The comparison for the natural frequency values of three beams B1 ÷ B3 according to three solutions (1) ÷ (3) is shown in Table 2. In Table 2, $BL_1$, $BL_2$, $BL_3$ are symbols of the first, second, and third lateral bending mode; $BV_1$, $BV_2$ are symbols of the first and second vertical bending mode and $T_1$, $T_2$, $T_3$, $T_4$, $T_5$ are symbols of the first, second, third, fourth and fifth torsional mode, respectively.

**Table 2.** Comparison of natural frequency $\omega$ for three beams B1 ÷ B3 (steel I-girder with trapezoidal web corrugations)

| Model /mode | | ABAQUS (FEM-S4R-shell-element) (rad/s) | Authors (FEM -7DOFs-beam -element) (rad/s) | The differences (%) | Authors (proposed formulas) (rad/s) | The differences (%) |
|---|---|---|---|---|---|---|
| | | | | (3) and (2) | | (5) and (3) |
| B1 | $BL_1$ | 26.580 | 26.754 | 0.657 | 26.754 | 0.000 |
| | $BL_2$ | 105.840 | 106.935 | 1.034 | 106.935 | 0.000 |
| | $BL_3$ | 235.676 | 240.294 | 1.959 | 240.292 | -0.001 |
| | $BV_1$ | 111.621 | 123.012 | 10.205 | N/A | N/A |
| | $BV_2$ | 393.861 | 484.093 | 22.909 | N/A | N/A |

| Model /mode | | ABAQUS (FEM-S4R-shell-element) (rad/s) | Authors (FEM -7DOFs-beam - element) (rad/s) | The differences (%) (3) and (2) | Authors (proposed formulas) (rad/s) | The differences (%) (5) and (3) |
|---|---|---|---|---|---|---|
| | $T_1$ | 35.127 | 35.039 | -0.252 | 34.488 | -1.572 |
| | $T_2$ | 121.881 | 122.568 | 0.564 | 119.769 | -2.284 |
| | $T_3$ | 264.202 | 267.463 | 1.234 | 260.698 | -2.529 |
| | $T_4$ | 459.489 | 469.484 | 2.175 | 457.848 | -2.478 |
| | $T_5$ | 696.177 | 727.960 | 4.565 | 708.643 | -2.653 |
| B2 | $BL_1$ | 26.516 | 26.861 | 1.300 | 26.861 | 0.000 |
| | $BL_2$ | 105.658 | 107.360 | 1.611 | 107.360 | 0.000 |
| | $BL_3$ | 235.871 | 241.247 | 2.279 | 241.245 | -0.001 |
| | $BV_1$ | 110.622 | 123.894 | 11.998 | N/A | N/A |
| | $BV_2$ | 389.966 | 487.387 | 24.982 | N/A | N/A |
| | $T_1$ | 35.614 | 35.057 | -1.566 | 34.793 | -0.752 |
| | $T_2$ | 122.434 | 122.940 | 0.414 | 121.112 | -1.487 |
| | $T_3$ | 264.510 | 268.443 | 1.487 | 263.709 | -1.764 |
| | $T_4$ | 459.935 | 471.308 | 2.473 | 463.494 | -1.658 |
| | $T_5$ | 702.711 | 730.855 | 4.005 | 717.039 | -1.890 |
| B3 | $BL_1$ | 26.426 | 27.009 | 2.209 | 27.009 | 0.000 |
| | $BL_2$ | 105.319 | 107.952 | 2.501 | 107.952 | 0.000 |
| | $BL_3$ | 235.330 | 242.574 | 3.078 | 242.573 | -0.001 |
| | $BV_1$ | 109.654 | 125.117 | 14.101 | N/A | N/A |
| | $BV_2$ | 385.838 | 491.955 | 27.503 | N/A | N/A |
| | $T_1$ | 36.261 | 35.081 | -3.255 | 35.419 | 0.965 |
| | $T_2$ | 123.119 | 123.441 | 0.261 | 123.834 | 0.319 |
| | $T_3$ | 264.849 | 269.759 | 1.854 | 269.856 | 0.036 |
| | $T_4$ | 460.111 | 473.759 | 2.966 | 474.718 | 0.202 |
| | $T_5$ | 704.282 | 734.745 | 4.325 | 734.137 | -0.083 |

The natural frequency values of the FEM-7DOFs-beam-element and the FEM-S4R-shell-element show very good agreement in the first three BL-lateral bending modes as well as the first five T-torsional modes. The differences between the values of FEM-7DOFs-beam-element and FEM-S4R-shell-element are quite small in the early modes (+0.66% for $BL_1$ and -0.25% for $T_1$ of B1 beam; +1.30% for $BL_1$ and -1.57% for $T_1$ of B2 beam; +2.21% for $BL_1$ and -3.26% for $T_1$ of B3) and increase gradually in the following modes (+1.96% for $BL_3$ and +4.57% for $T_5$ of B1 beam; +2.28% for $BL_3$ and +4.01% for $T_5$ of B2 beam; +3.08% for $BL_3$ and +4.33% for $T_5$ of B3). This can be attributed to the fact that the higher modes obtained by a shell element FEM-S4R do not correspond to the beam kinematics any more, i.e. they imply deformations of the cross-section.

The natural frequency values of the FEM-7DOFs-beam-element are almost all greater than the natural frequency values of the FEM-S4R-shell-element because the beam element is stiffer than the shell element. The differences between the values of FEM-7DOFs-beam-element and FEM-S4R-shell-element in the BV-vertical bending modes are quite large (+10.21% for $BV_1$ and +22.91% for $BV_2$ of B1 beam; 12.00% for $BV_1$ and +24.98% for $BV_2$ of B2 beam; +14.10% for $BV_1$ and +27.50% for $BV_2$ of B3).

Furthermore, the comparison of the natural frequency values between the proposed formulas and FEM-7DOFs-beam-element is very good with only the difference of -0.001% for $BL_3$-mode of all three beams B1 ÷ B3, while for $T_5$-torsional mode the differences are -2.65% for B1, -1.89% for B2 and -0.08% for B3. Therefore, the proposed Eqs. (20) and (21) are highly reliable and can be applied to calculate the natural frequency for steel I-girder with trapezoidal web corrugations.

## 5. Concluding remarks

The natural frequency values of steel I-girder with trapezoidal web corrugations using FEM-7DOFs beam element and FEM-S4R shell element have very good similarities in the first lateral bending and torsional modes. The differences between two finite element models increase in high modes due to the combination of multiple modes using the FEM-S4R shell element model.

The natural frequency values of steel I-girder with trapezoidal web corrugations using the proposed formulas give very good results compared to the finite element methods and can be applied to predict eigenfrequencies.

## References

Abbas, H. H. (2003). Analysis and design of corrugated web I-girders for bridges using high performance steel. Ph.D. dissertation, Lehigh University, Bethlehem, Pa.

Inaam, Q., & Upadhyay, A. (2020). Behavior of corrugated steel I-girder webs subjected to patch loading: Parametric study. Journal of Constructional Steel Research, 165, 1058-1096.

Jager, B., Dunai, L., & Kövesdi, B. (2017). Flange buckling behavior of girders with corrugated web Part I: Experimental study. Thin-walled Structures, 118, 181-195.

Kang, Y. J., & Yoo, C. H. (1994). Thin-walled curved beams. I: Formulation of nonlinear equations. Journal of Engineering Mechanics, 120(10), 2072-2101.

Kang, Y. J., & Yoo, C. H. (1994). Thin-walled curved beams. II: Analytical solutions for buckling of arches. Journal of Engineering Mechanics, 120(10), 2102-2125.

Kövesdi, B., Jager, B., & Dunai, L. (2016). Bending and shear interaction behavior of girders with trapezoidally corrugated webs. Journal of Constructional Steel Research, 121, 383-397.

Lin, X., Far, H., & Ali Saleh. (2019). Structural Behaviour and Mechanical Properties of Welded Steel I-Girders with Corrugated Webs. International Journal of Steel Structures, 19(4), 1342-1352.

Lindner, J. (1990). Lateral torsional buckling of beams with trapezoidally corrugated webs. Stab Steel Struct Budapest, Hungary, 305-310.

Moon, J., Yi, J., Choi, B. H., & Lee, H. E. (2009). Shear strength and design of trapezoidally corrugated steel webs. Journal of Constructional Steel Research, 65(5), 1198-1205.

Nguyen, N. N., Kim, S. N., Han, S. R., & Kang, Y. J. (2010). Elastic lateral-torsional buckling strength of I-girder with trapezoidal web corrugations using a new warping constant under uniform moment. Engineering Structures, 32, 2157-2165.

Nguyen, V. H., Ton-That, H. L., Chau, D. T., & Dao, D. N. (2017). Nonlinear Static Bending Analysis of Functionally Graded Plates Using MISQ24 Elements with Drilling Rotations. International Conference on Advances in Computational Mechanics, ACOME, Springer, Singapore, 461-475.

Riahi, F., Behravesh, A., Fard, M. Y., & Armaghani, A. (2018). Shear Buckling Analysis of Steel Flat and Corrugated Web I-girders. KSCE Journal of Civil Engineering, 22, 5058-5073.

Say-Ahmed, E. Y. (2005). Lateral torsion–flexure buckling of corrugated web steel girders. Proceedings of the Institution of Civil Engineers - Structures and Buildings, 158(1), 53-69.

Ton, T. H. L. (2020). A new C0 third-order shear deformation theory for the nonlinear free vibration analysis of stiffened functionally graded plates. Facta Universitatis, Series: Mechanical Engineering, DOI: 10.22190/FUME200629040T.

Ton, T. H. L., Nguyen, V. H., & Chau, D. T. (2020). An Improved Four-Node Element for Analysis of Composite Plate/Shell Structures Based on Twice Interpolation Strategy. International Journal of Computational Methods, 17(6), 1950-1990.

Ton, T. H. L., Nguyen, V. H., & Chau, D. T. (2020). Nonlinear Bending Analysis of Functionally Graded Plates Using SQ4T Elements based on Twice Interpolation Strategy. Journal of Applied and Computational Mechanics, 6(1), 125-136.

Ton, T. H. L., Nguyen, V. H., Chau, D. T., & Huynh. V. C. (2018). Enhancement to four-node quadrilateral plate elements by using cell-based smoothed strains and higher-order shear deformation theory for nonlinear analysis of composite structures. Journal of Sandwich Structures & Materials, 22(7), 2302-2329.